Theoretical study on photorecombination of C V ion*

Ma Kun(马 堃)[a)b)], Xie Lu-You(颉录有)[a)], Zhang Deng-Hong(张登红)[a)], and Dong Chen-Zhong(董晨钟)[a)†]

[a)] *Key Laboratory of Atomic and Molecular Physics & Functional Materials of Gansu Province, College of Physics and Electronic Engineering, Northwest Normal University, Lanzhou* 730070, *China*

[b)] *School of Information Engineering, Huangshan University, Huangshan* 245041, *China*

(Received 21 October 2014; revised manuscript received 3 January 2015; published online 29 May 2015)

The partial and total photorecombination cross sections of the ground-state C V ion in the KLL and KLM resonant energy regions were calculated in detail by using the Dirac atomic *R*-matrix code based on a fully relativistic *R*-matrix method. Meanwhile, the principal resonant lines in each photorecombination channel have been classified according to the calculated transition energies and probabilities from the KLL and KLM resonant states to the $1s^2nl$ ($n = 2$, 3 and $l = s, p, d$) final states. The validity of these calculations is assessed by comparison with previously published experimental and theoretical data. The good agreement between the present calculated results and those obtained using different approaches confirms the accuracy of the present results. In addition, it is found that the damping effect can be neglected for the KLL resonant, but not for the KLM resonant.

Keywords: photorecombination, *R*-matrix method, C V ion

PACS: 34.80.Lx, 34.10.+x **DOI:** 10.1088/1674-1056/24/7/073402

1. Introduction

Photorecombination (PR) process is an important atomic process of interest in applied and fundamental physics.[1] This process may seriously affect the ionization balance and ionic excited-state distributions of laboratory and astronomical plasmas, as in fusion devices and in the solar corona, and it is also an important cooling mechanism of high-temperature plasmas.[2,3] The PR process is generally treated as two independent processes. One process is a direct PR, i.e., the radiative recombination (RR) process, which is a direct transition from a free to a bound state with the emission of a photon. The other process is the well-known resonant PR, i.e., the dielectronic recombination (DR) process, which is the resonant capture of an electron by an ion followed by radiative stabilization through emission of one or more photons. However, from the point of view of quantum mechanics, all the PR processes, including RR and DR, can interfere near the resonance position if the initial and final atomic states are the same.

Theoretically, nonperturbative and perturbative approaches are used to investigate the PR process. The advantage of nonperturbative approach is that it automatically includes any quantum-mechanical interference between the resonant part (DR) and the nonresonant part (RR), the drawback is that it normally omits radiation damping. Although radiation damping is easily included by perturbative approach,[4–6] it is impracticable to include all the perturbative orders in practical calculations. In view of the above, nonperturbative approaches, such as the close-coupling *R*-matrix theories of Burke, Hibbert, and Robb,[7,8] are used in the present paper. Nahar and Pradhan[9–11] pointed out that the photoionization (PI) cross sections calculated in the close-coupling approximation and by the *R*-matrix method may be employed to treat the PR process without the physically artificial distinction between the DR and RR processes. Then, a series works[6,12–19] have been reported on a PR process based on the method and good results have been obtained. In Zhao *et al.*'s work,[6] they presented a numerical method to calculate the low-lying resonance PR by evaluating the Cauchy principal value of the integral in scattering matrices directly. This method was developed within the framework of the rigorous continuum-bound transition of Davies and Seaton,[20] and the radiation damping effect could be considered simply. In the experimental aspect, the DR and RR interferences in highly charged U ($Z = 92$) ions have been observed at the super-EBIT facility of the Lawrence Livermore National Laboratory,[21] and then the interference was also observed for Hg ($Z = 80$) ions with the Heidelberg EBIT[22] and for Bi ($Z = 83$) ions with the Tokyo EBIT.[23,24]

In the present work, based on the work of Nahar and Pradhan, the PR process of C V ion in the low-lying resonant energy regions have been studied by using the Dirac atomic *R*-matrix code (DARC)[25] based on a fully relativistic *R*-matrix method. Firstly, the PI cross sections from C IV ground state and excited state to C V ground state are calculated by DARC. Then, the PR cross sections of C V ion in the ground state can be obtained based on the principle of detailed balance. The advantage of this method is that it can automatically include the interference of DR and RR processes, and a fully relativistic *R*-matrix method could include more detailed resonant structure.

*Project supported by the National Natural Science Foundation of China (Grant Nos. 11274254, U1332206, and U1331122) and the International Scientific and Technological Cooperative Project of Gansu Province, China (Grant No. 1104WCGA186).

†Corresponding author. E-mail: dongcz@nwnu.edu.cn

© 2015 Chinese Physical Society and IOP Publishing Ltd

In addition, for identifying the principal resonant lines in each PR channel, the transition energies and probabilities from the KLL and KLM resonant states to $1s^2nl$ ($n = 2$, 3 and $l = s, p, d$) states have been calculated by GRASP2K[26,27] and RATIP[28] package based on the multiconfiguration Dirac–Fock (MCDF) method.

The remainder of this paper is organized as follows. In Section 2, the theoretical method is described briefly. In Section 3, the target energies, resonant energies, and the PR cross sections of C V ion in the KLL and KLM resonant energy regions are given. Finally in Section 4 conclusions are drawn.

2. Theoretical method

In this paper, the close-coupling approximation and the fully relativistic R-matrix method are employed to study the PR process. Here we present a brief description of the theory relevant to the calculations of PR cross sections.

2.1. R-matrix for photoionization

The PI process could be expressed as

$$h\nu + A^{q+} \rightarrow A^{(q+1)+} + e^-, \tag{1a}$$

$$h\nu + A^{q+} \rightarrow (A^{q+})^* \rightarrow A^{(q+1)+} + e^-. \tag{1b}$$

Equation (1a) denotes the direct PI and equation (1b) denotes the resonant PI. The Dirac–Coulomb Hamiltonian for the $(N+1)$-electron system of the initial PI process can be expressed in atomic units as

$$H^{N+1} = \sum_{i=1}^{N+1} -ic\alpha\nabla_i + (\beta - 1)c^2 - \frac{Z}{r_i} + \sum_{j=i+1}^{N+1} \frac{1}{|\boldsymbol{r}_j - \boldsymbol{r}_i|}, \tag{2}$$

where i and j denote the individual electrons index, and α and β are the Dirac matrices. The first three one-electron terms on the right-hand side in the Hamiltonian are the momentum term, the mass term, and the electron–nucleus Coulomb attraction, respectively. The final two-electron term represents the Coulomb electron–electron repulsion.

The R-matrix theory divides configuration space into an inner and an outer region, separated by a spherical shell of radius r_a centred at the nucleus. In the inner region, all $N+1$ electrons are treated on an equal footing and all exchange effects are considered. The $(N+1)$-electron wave function for the J^π symmetry is given by

$$\begin{aligned}&\psi_k(x_1, x_2, \ldots, x_{N+1}) \\ &= A\sum_{ij} c_{ijk}\bar{\Phi}_i(x_1, x_2, \ldots, x_N; \hat{r}_{N+1}\sigma_{N+1})\frac{1}{r_{N+1}}u_{ij}(r_{N+1}) \\ &\quad + \sum_j d_{jk}\phi_j(x_1, x_2, \ldots, x_{N+1}),\end{aligned} \tag{3}$$

where $\bar{\Phi}_i$ are the target state wave functions coupled with the angular and spin parts of the incoming electron, A is the antisymmetry operator, u_{ij} is the continuum wave function of a free electron, and ϕ_j is the $(N+1)$-electron bound state wave function. The summation over i, j of the first term is over all open channels of $\bar{\Phi}_i$ and over all continuum electronic orbital u_{ij} to meet the J^π symmetry. The summation over j of the second term is over all $(N+1)$-electron bound states to ensure the completeness of the basis. In the outer region, the system is simplified as a two-body system where the incoming electron is in a long-range multipole field. The wave functions in this region is given by

$$\begin{aligned}&\psi_k(x_1, x_2, \ldots, x_{N+1}) \\ &= \sum_{ij} c_{ijk}\bar{\Phi}_i(x_1, x_2, \ldots, x_N; \hat{r}_{N+1}\sigma_{N+1})\frac{1}{r_{N+1}}u_{ij}(r_{N+1}).\end{aligned} \tag{4}$$

The parameters c_{ijk} and d_{jk} are calculated by diagonalizing the $(N+1)$-electron Hamiltonian within the inner region of the R-matrix box. Then enforcing continuity at the boundary, we obtain the wavefunction in both regions with the R-matrix as a connection between the parts.

In Eqs. (3) and (4), the relativistic electron wavefunction has the form of

$$\varphi(r) = \frac{1}{r}\begin{pmatrix} P_{n\kappa}(r)\chi^m_\kappa(\theta, \phi) \\ iQ_{n\kappa}(r)\chi^m_{-\kappa}(\theta, \phi) \end{pmatrix}, \tag{5}$$

where $P_{n\kappa}(r)$ and $Q_{n\kappa}(r)$ are the large and small component radial wave functions, respectively, the functions $\chi^m_\kappa(\theta, \phi)$ are the spin spherical harmonics, and κ is the relativistic angular quantum number of a continuum electron, $\kappa = \pm(j + \frac{1}{2})$ for $\ell = j \pm \frac{1}{2}$.

The PI cross-section can be expressed in dipole length form as

$$\sigma_{PI} = \frac{4\pi^2 a_0^2 \alpha}{3}\frac{\omega}{g}S_L, \tag{6}$$

where g is the statistical weight of the initial state and S_L is the generalized line strength, which include not only direct PI and resonant PI process, but also the interference of these two processes.[25]

In the present PI calculations, the continuum orbital with different angular momentum is expressed as a linear combination of 25 numerical basis functions. To resolve the fine resonant structure in the respective PR cross sections, a suitably chosen fine energy mesh of 10^{-4} Ryd between the thresholds has been adopted.

2.2. R-matrix for photorecombination

Recombination of an incoming electron to the ground state of C V ion may occur through non-resonant background continuum, usually referred to as RR,

$$e^- + C^{4+}(1s^2) \rightarrow C^{3+}(1s^2 n\ell) + h\nu, \tag{7}$$

which is the inverse process of the direct PI, or through a two-step recombination process, i.e., dielectronic recombination (DR),

$$e^- + C^{4+}(1s^2) \rightarrow C^{3+}(1snl n'l') \rightarrow C^{3+}(1s^2 n''l'') + h\nu, \quad (8)$$

which is the inverse process of the resonant PI.

According to the principle of detailed balance (Milne relation), the relationship between the PR and PI cross-sections can be obtained as

$$\sigma_{PR}(\varepsilon) = \frac{\alpha^2}{4}\frac{g_f}{g_i}\frac{(\varepsilon + I)^2}{\varepsilon}\sigma_{PI}, \quad (9)$$

where α is the fine structure constant, ε is the photoelectron energy, I is the ionization potential, and $g_i(g_f)$ is the statistical weight of the recombined initial (final) state.

3. Calculation and discussion

3.1. Target state energies

The target state wavefunction of C V ions are described by 23 relativistic orbits: $1s_{1/2}$, $2s_{1/2}$, $2p_{1/2}$, $2p_{3/2}$, $3s_{1/2}$, $3p_{1/2}$, $3p_{3/2}$, $3d_{3/2}$, $3d_{5/2}$, $4s_{1/2}$, $4p_{1/2}$, $4p_{3/2}$, $4d_{3/2}$, $4d_{5/2}$, $4f_{7/2}$, $4f_{9/2}$, $5s_{1/2}$, $5p_{1/2}$, $5p_{3/2}$, $5d_{3/2}$, $5d_{5/2}$, $5f_{7/2}$, $5f_{9/2}$. All of these orbits are obtained by using the EOL scheme. In the RSCF of the GRASP2K[26,27] and DSTG2 of the DARC[25] calculations, the target wavefunctions are generated by $1snl$ ($n = 1, 2, 3, 4, 5$, $l = s, p, d, f$), and their lowest 17 levels are included in the generation of channels.

Table 1 lists the target state energies of C V ion along with the data from the NIST database[29] for comparison. It can be seen that the energies calculated by MCDF agree well with DARC results for all of the above mentioned target states. However, there is about a 1 eV discrepancy between our results and NIST. This discrepancy is mainly caused by the remained electron correlation effects.

Table 1. The lowest seventeen energy levels in C V ion (in eV).

No.	Target	J	DARC	MCDF	NIST
1	$1s^2$	0	0	0	0
2	1s2s	1	297.95	297.95	298.96
3	1s2s	0	303.55	303.55	304.38
4	$1s2p_{1/2}$	1	303.47	303.47	304.40
5	$1s2p_{1/2}$	0	303.46	303.46	304.40
6	$1s2p_{3/2}$	2	303.49	303.49	304.42
7	$1s2p_{3/2}$	1	307.01	307.01	307.90
8	1s3s	1	351.02	351.02	352.06
9	1s3s	0	352.53	352.53	353.50
10	$1s3p_{1/2}$	1	352.50	352.50	353.53
11	$1s3p_{1/2}$	0	352.50	352.50	353.53
12	$1s3p_{3/2}$	2	352.51	352.51	353.53
13	$1s3d_{3/2}$	1	353.21	353.21	354.26
14	$1s3d_{3/2}$	2	353.21	353.21	354.26
15	$1s3d_{5/2}$	3	353.21	353.21	354.26
16	$1s3d_{5/2}$	2	353.24	353.24	354.29
17	$1s3p_{3/2}$	1	353.51	353.51	354.52

3.2. Transition energies and probabilities

Transition energies and transition probabilities of KLL and KLM resonant states to PR final state have been calculated by the component (REOS) of the RATIP package[28] and the results have been listed in Table 2, in which B and C denote the transition probabilities in Babushkin and Coulomb gauges, respectively. For the sake of simplicity, these resonant transition lines are ordered as a number, which are listed in the 'Label' column of Table 2. It can be seen that the transition probabilities of the most lines listed in this table are in good agreement in the two different gauges, however, there is a relative lager divergence for some weaker transition lines, such as the transitions 53, 54, 65, 81, 87, 98, and 118. In fact, in these transition processes, the two electrons change and one photon emits simultaneously, which is the so-called TEOP transitions.[30–33] For example, the transition 53 corresponds to the $(1s2s)_0 3p_{3/2}$ $J = 1/2$ to the $1s^2 3s$ $J = 1/2$ transition. The TEOP process was first theoretically predicted by Heisenberg[33] and it is mainly caused by strong configuration interactions. As can be seen from Table 2, the transition probabilities of these TEOP processes are relatively small in the present work.

Table 2. Transition energies and probabilities from the KLL and KLM resonant states to the PR final states.

Label	Resonant state		Energy/eV	$A_r/10^9$ s^{-1}		Label	Resonant state		Energy/eV	$A_r/10^9$ s^{-1}	
	Configuration	J		C	B		Configuration	J		C	B
	KLL and KLM resonant state $\rightarrow 1s^2 2s$ $J = 1/2$					65	$1s2s^2$	1/2	249.978	0.325	0.071
1	$[1s2s]_0 2p_{1/2}$	1/2	298.67	765.8	754.2	66	$[1s2p_{1/2}]_0 3p_{1/2}$	3/2	265.84	4.196	2.510
2	$[1s2s]_0 2p_{3/2}$	3/2	298.75	783.4	769.5	67	$[1s2p_{1/2}]_1 2p_{3/2}$	1/2	267.11	6.354	6.120
3	$[1s2s]_0 3p_{3/2}$	1/2	302.03	90.85	84.20	68	$1s[2p^2_{3/2}]_2$	3/2	267.22	1.346	1.337
4	$[1s2s]_1 2p_{3/2}$	3/2	302.04	73.72	69.17	69	$1s[2p^2_{3/2}]_0$	1/2	272.16	0.603	0.468
5	$[1s2s]_1 3p_{1/2}$	3/2	333.71	2.882	2.888	70	$[1s2s]_1 3s$	1/2	293.26	0.119	0.068
6	$[1s2s]_1 3p_{3/2}$	3/2	334.03	153.4	131.6	71	$[1s2s]_1 3d_{5/2}$	3/2	297.00	0.596	0.787
7	$[1s2s]_1 3p_{3/2}$	1/2	334.07	163.0	137.8	72	$[1s2s]_0 3s$	1/2	297.77	24.48	22.61
8	$[1s2s]_0 3p_{1/2}$	1/2	338.92	73.94	51.65	73	$[1s2p_{1/2}]_1 3p_{3/2}$	1/2	299.65	4.846	4.869
9	$[1s2s]_0 3p_{3/2}$	3/2	338.93	74.10	50.33	74	$[1s2p_{3/2}]_2 3p_{3/2}$	3/2	299.90	6.426	7.133
10	$[1s2p_{1/2}]_1 3s$	1/2	340.25	5.150	7.155	75	$[1s2p_{3/2}]_1 3p_{1/2}$	1/2	299.93	23.87	25.94
11	$[1s2p_{3/2}]_2 3s$	3/2	340.38	8.596	10.08	76	$[1s2p_{1/2}]_1 3p_{3/2}$	3/2	301.58	99.71	105.2
12	$[1s2p_{3/2}]_1 3s$	1/2	342.19	18.34	31.63	77	$[1s2s]_0 3d_{3/2}$	3/2	302.12	8.830	6.019

Table 2. (*Continued*).

Label	Resonant state		Energy/eV	$A_r/10^9$ s^{-1}		Label	Resonant state		Energy/eV	$A_r/10^9$ s^{-1}	
	Configuration	J		C	B		Configuration	J		C	B
	KLL and KLM resonant state $\rightarrow 1s^2 2p_{1/2}$ $J = 1/2$					78	$[1s2p_{3/2}]_2 3p_{3/2}$	1/2	303.03	25.98	29.13
13	$1s2s^2$	1/2	280.84	14.93	14.14	79	$[1s2p_{3/2}]_1 3p_{1/2}$	3/2	303.84	756.4	659.2
14	$[1s2p_{1/2}]_0 3p_{1/2}$	3/2	296.70	360.4	339.3	80	$[1s2p_{3/2}]_1 3p_{1/2}$	1/2	303.94	647.3	540.5
15	$[1s2p_{1/2}]_1 2p_{3/2}$	1/2	297.97	850.1	830.5		KLL and KLM resonant state $\rightarrow 1s^2 3p_{3/2}$ $J = 3/2$				
16	$1s[2p^2_{3/2}]_2$	3/2	298.08	187.8	183.1	81	$1s2s^2$	1/2	249.54	0.717	0.117
17	$1s[2p^2_{3/2}]_0$	1/2	303.02	103.8	106.0	82	$[1s2p_{1/2}]_1 2p_{3/2}$	5/2	265.38	5.535	3.473
18	$[1s2s]_1 3s$	1/2	324.12	2.220	2.659	83	$[1s2p_{1/2}]_0 3p_{1/2}$	3/2	265.41	0.671	0.380
19	$[1s2s]_1 3d_{5/2}$	3/2	327.86	15.48	14.85	84	$[1s2p_{1/2}]_1 2p_{3/2}$	1/2	266.67	3.548	3.370
20	$[1s2s]_0 3s$	1/2	328.56	5.492	5.672	85	$1s[2p^2_{3/2}]_2$	3/2	266.78	9.261	8.800
21	$[1s2p_{1/2}]_1 3p_{3/2}$	1/2	330.33	53.89	39.56	86	$1s[2p^2_{3/2}]_0$	1/2	271.72	1.650	1.236
22	$[1s2p_{1/2}]_0 3p_{1/2}$	1/2	330.48	1.644	1.530	87	$[1s2s]_1 3s$	1/2	292.83	0.239	0.094
23	$[1s2p_{3/2}]_2 3p_{3/2}$	3/2	330.76	29.03	24.48	88	$[1s2s]_1 3d_{3/2}$	5/2	296.54	0.529	0.706
24	$[1s2p_{3/2}]_1 3p_{1/2}$	1/2	330.79	117.0	96.77	89	$[1s2s]_1 3d_{5/2}$	3/2	296.57	0.104	0.143
25	$[1s2p_{1/2}]_1 3p_{3/2}$	3/2	332.44	124.5	102.3	90	$[1s2s]_0 3s$	1/2	297.27	46.34	41.51
26	$[1s2s]_0 3d_{3/2}$	3/2	332.98	72.07	50.03	91	$[1s2p_{3/2}]_2 3p_{3/2}$	3/2	299.46	29.32	32.03
27	$[1s2p_{3/2}]_2 3p_{3/2}$	1/2	333.89	84.33	63.92	92	$[1s2p_{3/2}]_1 3p_{1/2}$	1/2	299.49	11.39	12.16
28	$[1s2p_{3/2}]_1 3p_{1/2}$	3/2	334.52	102.2	95.93	93	$[1s2p_{1/2}]_1 3p_{3/2}$	3/2	301.15	21.43	22.80
	KLL and KLM resonant state $\rightarrow 1s^2 2p_{3/2}$ $J = 3/2$					94	$[1s2p_{1/2}]_1 3p_{3/2}$	5/2	301.19	106.6	112.4
29	$1s2s^2$	1/2	280.60	28.99	27.05	95	$[1s2s]_0 3d_{5/2}$	5/2	301.68	15.98	12.12
30	$[1s2p_{1/2}]_1 2p_{3/2}$	5/2	296.43	395.8	375.4	96	$[1s2p_{3/2}]_2 3p_{3/2}$	1/2	302.60	67.64	76.82
31	$[1s2p_{1/2}]_0 3p_{1/2}$	3/2	296.47	45.75	42.09	97	$[1s2p_{3/2}]_1 3p_{3/2}$	5/2	304.20	717.1	705.3
32	$[1s2p_{1/2}]_1 2p_{3/2}$	1/2	297.73	409.1	399.8		KLL and KLM resonant state $\rightarrow 1s^2 3d_{3/2}$ $J = 3/2$				
33	$1s[2p^2_{3/2}]_2$	3/2	297.84	1073	1046	98	$[1s2s]_0 2p_{1/2}$	1/2	258.81	0.135	0.270
34	$1s[2p^2_{3/2}]_0$	1/2	302.78	236.2	237.8	99	$[1s2s]_0 2p_{3/2}$	3/2	258.88	0.011	0.019
35	$[1s2s]_1 3s$	1/2	323.89	4.384	5.100	100	$[1s2s]_0 3p_{3/2}$	1/2	262.16	1.854	1.969
36	$[1s2s]_1 3d_{3/2}$	5/2	327.60	17.81	17.18	101	$[1s2s]_1 2p_{3/2}$	3/2	262.17	0.185	0.190
37	$[1s2s]_1 3d_{5/2}$	3/2	327.62	3.018	2.868	102	$[1s2s]_0 3p_{1/2}$	1/2	299.06	26.82	26.89
38	$[1s2s]_0 3s$	1/2	328.33	10.31	11.62	103	$[1s2s]_0 3p_{3/2}$	3/2	299.06	2.671	2.704
39	$[1s2p_{1/2}]_1 3p_{1/2}$	3/2	330.26	1.346	1.155	104	$[1s2p_{1/2}]_1 3s$	1/2	300.38	3.063	2.318
40	$[1s2p_{1/2}]_1 3p_{3/2}$	1/2	330.48	23.33	37.96	105	$[1s2p_{3/2}]_2 3d_{5/2}$	5/2	301.09	1.103	1.167
41	$[1s2p_{3/2}]_2 3p_{3/2}$	3/2	330.52	140.0	116.4	106	$[1s2p_{3/2}]_2 3d_{5/2}$	3/2	301.09	8.433	8.196
42	$[1s2p_{3/2}]_1 3p_{1/2}$	1/2	330.55	58.76	47.81	107	$[1s2p_{3/2}]_1 3s$	3/2	302.26	1.304	1.777
43	$[1s2p_{3/2}]_1 3p_{3/2}$	3/2	331.02	1.384	1.007	108	$[1s2p_{1/2}]_1 3d_{5/2}$	5/2	302.29	95.46	92.40
44	$[1s2p_{1/2}]_1 3p_{3/2}$	3/2	332.21	27.12	22.72	109	$[1s2p_{3/2}]_1 3s$	1/2	302.32	40.01	40.52
45	$[1s2p_{1/2}]_1 3p_{3/2}$	5/2	332.24	162.4	133.2	110	$[1s2p_{3/2}]_2 3d_{5/2}$	1/2	303.25	20.09	17.53
46	$[1s2s]_0 3d_{5/2}$	5/2	332.74	67.97	46.30	111	$[1s2p_{3/2}]_1 3d_{3/2}$	5/2	305.62	364.1	356.9
47	$[1s2s]_0 3d_{3/2}$	3/2	332.74	15.56	10.68	112	$[1s2p_{3/2}]_1 3d_{5/2}$	5/2	305.66	448.4	434.3
48	$[1s2p_{3/2}]_2 3p_{3/2}$	1/2	333.66	175.1	134.0	113	$[1s2p_{3/2}]_1 3d_{3/2}$	3/2	305.76	841.3	732.0
49	$[1s2p_{3/2}]_1 3p_{1/2}$	3/2	334.68	19.79	31.91	114	$[1s2p_{3/2}]_1 3d_{3/2}$	1/2	306.65	918.9	833.5
50	$[1s2p_{3/2}]_1 3p_{3/2}$	5/2	335.26	87.82	90.69	115	$[1s2p_{3/2}]_1 3d_{5/2}$	3/2	306.70	90.65	81.31
	KLL and KLM resonant state $\rightarrow 1s^2 3s$ $J = 1/2$						KLL and KLM resonant state $\rightarrow 1s^2 3d_{5/2}$ $J = 5/2$				
51	$[1s2s]_0 2p_{1/2}$	1/2	261.62	2.316	2.630	116	$[1s2s]_0 2p_{3/2}$	3/2	258.80	0.098	0.191
52	$[1s2s]_0 2p_{3/2}$	3/2	261.70	2.355	2.812	117	$[1s2s]_1 2p_{3/2}$	3/2	262.09	1.765	1.805
53	$[1s2s]_0 3p_{3/2}$	1/2	264.98	0.442	0.233	118	$[1s2s]_1 3p_{3/2}$	3/2	294.08	0.053	0.098
54	$[1s2s]_1 2p_{3/2}$	3/2	264.98	0.396	0.159	119	$[1s2s]_0 3p_{3/2}$	3/2	298.98	23.41	23.54
55	$[1s2s]_1 3p_{3/2}$	3/2	296.98	6.590	7.263	120	$[1s2p_{3/2}]_2 3s$	3/2	300.43	3.284	2.617
56	$[1s2s]_1 3p_{3/2}$	1/2	297.02	6.719	7.284	121	$[1s2p_{3/2}]_2 3d_{5/2}$	5/2	301.01	8.624	8.414
57	$[1s2s]_0 3p_{1/2}$	1/2	301.88	21.36	18.67	122	$[1s2p_{3/2}]_2 3d_{5/2}$	3/2	301.01	0.724	0.610
58	$[1s2s]_0 3p_{3/2}$	3/2	301.88	22.45	20.33	123	$[1s2p_{1/2}]_1 3d_{5/2}$	5/2	302.21	8.432	8.442
59	$[1s2p_{1/2}]_1 3s$	1/2	303.20	97.36	102.0	124	$[1s2p_{3/2}]_2 3d_{3/2}$	7/2	302.24	99.96	95.50
60	$[1s2p_{3/2}]_2 3s$	3/2	303.33	97.79	101.7	125	$[1s2p_{3/2}]_1 3s$	3/2	302.28	14.13	14.65
61	$[1s2p_{3/2}]_1 3s$	3/2	304.89	744.5	640.8	126	$[1s2p_{1/2}]_1 3d_{5/2}$	3/2	303.50	7.335	5.768
62	$[1s2p_{3/2}]_1 3s_{1/2}$	1/2	305.14	660.7	643.3	127	$[1s2p_{3/2}]_1 3d_{3/2}$	5/2	305.54	567.6	566.5
63	$[1s2p_{1/2}]_1 3d_{5/2}$	3/2	306.11	182.8	167.5	128	$[1s2p_{3/2}]_1 3d_{5/2}$	7/2	305.58	803.2	781.3
64	$[1s2p_{3/2}]_1 3d_{5/2}$	3/2	309.33	5.758	4.479	129	$[1s2p_{3/2}]_1 3d_{5/2}$	5/2	305.58	378.9	373.3
	KLL and KLM resonant state $\rightarrow 1s^2 3p_{1/2}$ $J = 1/2$					130	$[1s2p_{3/2}]_1 3d_{3/2}$	3/2	305.78	92.54	79.36
						131	$[1s2p_{3/2}]_1 3d_{5/2}$	3/2	306.72	823.1	744.7

3.3. The PR cross section

In this section, the PI cross sections of C IV ion from the $1s^2nl$ ($n = 2, 3$, $l =$ s, p, d) to the $1s^2$ have been calculated firstly by the DARC, and then the PR cross sections of C V ion from the $1s^2$ state to the $1s^2nl$ ($n = 2, 3$, $l =$ s, p, d) states will be obtained by the means of the principle of detailed balance. According to the J^π symmetry, there are two PR channels for the recombined states $1s^22s$, $1s^22p_{1/2}$, $1s^23s$, and $1s^23p_{1/2}$, three PR channels for the recombined states $1s^22p_{3/2}$, $1s^23p_{3/2}$, $1s^23d_{3/2}$, and $1s^23d_{5/2}$. Partial PR cross sections for each channel of these PR processes have been shown in Figs. 1–3. In these figures, the most of the distinguishable resonant lines have been labeled using the number in Table 2.

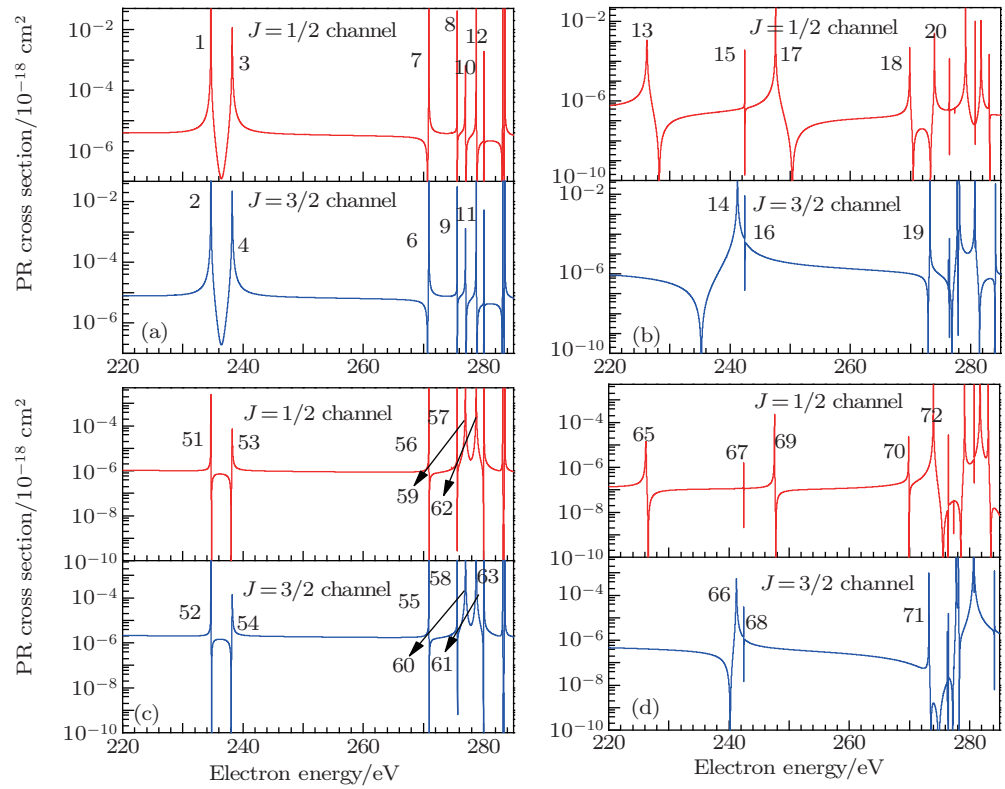


Fig. 1. (color online) Partial PR cross sections of C V from $1s^2$ to recombined states (a) $1s^22s$, (b) $1s^22p_{1/2}$, (c) $1s^23s$, and (d) $1s^23p_{1/2}$.

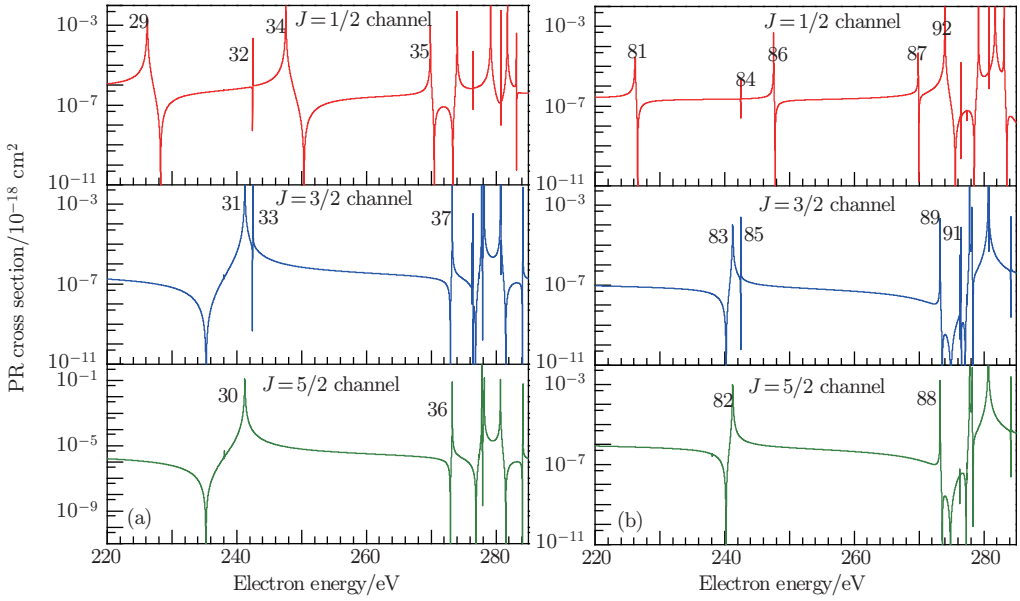


Fig. 2. (color online) Partial PR cross sections of C V from $1s^2$ to recombined states (a) $1s^22p_{3/2}$ and (b) $1s^23p_{3/2}$.

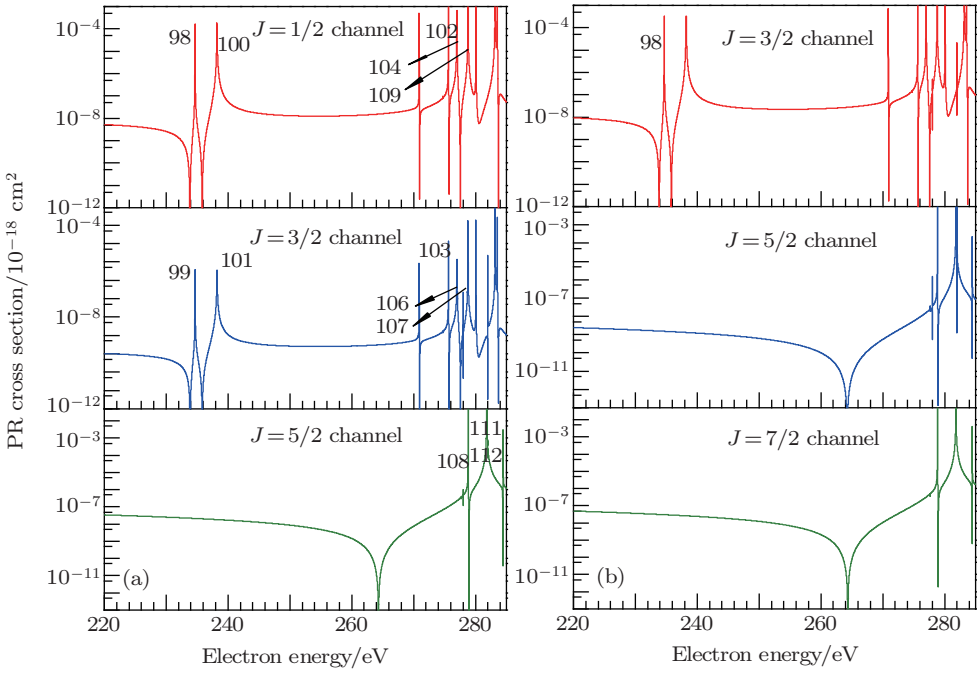


Fig. 3. (color online) Partial PR cross sections of C V from $1s^2$ to recombined states (a) $1s^23d_{3/2}$ and (b) $1s^23d_{5/2}$.

The total PR cross sections of C V from the $1s^2$ to the recombined states $1s^2nl$ ($n = 2$, 3, $l =$ s, p, d) have been shown in Fig. 4. From this figure, we can see that there is a close relationship between the profile of the PR cross sections and the orbital angular quantum of recombined orbital. For example, the profile of 2s is similar to 3s, $2p_{1/2}$ and $2p_{3/2}$ are similar to $3p_{1/2}$ and $3p_{3/2}$, and so on.

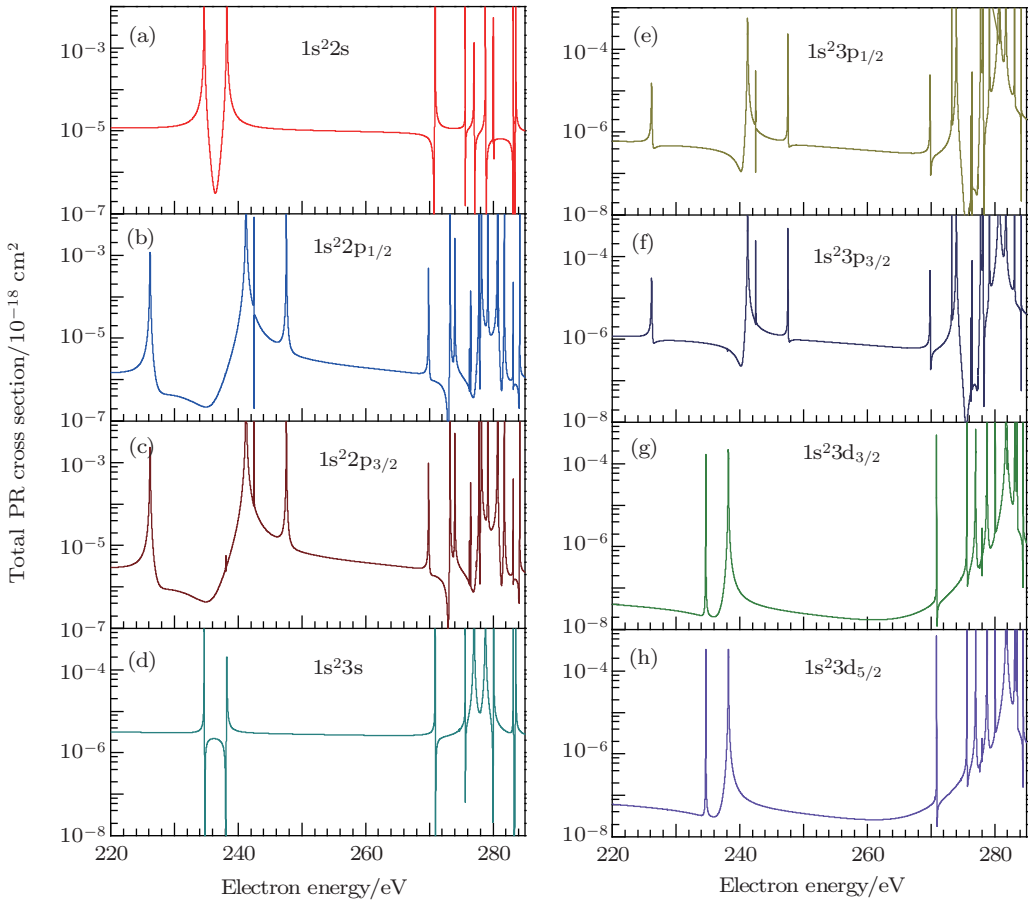


Fig. 4. (color online) Total PR cross sections of C V from $1s^2$ to recombined states (a) $1s^22s$, (b) $1s^22p_{1/2}$, (c) $1s^22p_{3/2}$, (d) $1s^23s$, (e) $1s^23p_{1/2}$, (f) $1s^23p_{3/2}$, (g) $1s^23d_{3/2}$, and (h) $1s^23d_{5/2}$.

In order to test the validity of the above calculated results, we further obtain the composite PR cross sections of the C V ion in the ground state by summing over the total PR cross sections for each recombined final state, such as the ground state and $1s^2nl$ ($n = 2$, 3, $l =$ s, p, d) excited states. Then, we compare with the experimental results from Mannervik[34] and Müller,[35] and the perturbative theoretical results from Zhao.[6] The present calculated results are convolved with FWHM = 0.65 eV in the Gaussian distribution. To match the experimental results, the calculated resonant positions by us and Zhao have been shifted 0.8 eV and 0.4 eV, respectively, and the calculated cross sections have been shifted 0.4×10^{-20} cm^2. As shown in Fig. 5, there is a very good agreement for both the amplitude of the cross sections and the line shapes. However, there is a little discrepancy for the KLM resonant intensity. The present results are similar to Zhao's undamping results. However, Zhao's damping results reduce the KLM resonant intensity and better agree with the experimental results. Therefore, we can say that the damping effect is important for the KLM resonant, but not for the KLL resonant.

According to Pradhan *et al.*,[36] the radiation damping contributions to the PR process depend on the ratio between the radiation width (Γ_r) and the total width ($\Gamma = \Gamma_r + \Gamma_a$), where Γ_a denotes the Auger width. In Table 3, the radiation and Auger widths of the KLL and KLM resonant states for C IV ion have been presented by the flexible atomic code (FAC).[37] As can be seen from this table, the radiation widths increase with the increase of energies of the resonant excited states. For example, for the resonant state $1s2s^2$, the ratio Γ_r/Γ is 0.001%, but is 26.57% for the 1s2p3d state.

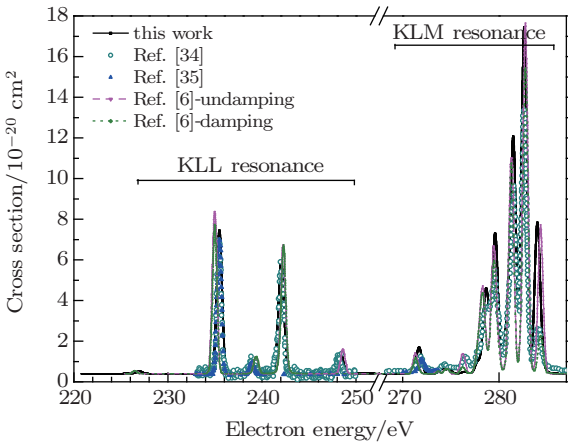


Fig. 5. (color online) The PR cross sections of C V ion in KLL and KLM resonant regions.

Table 3. Radiation and Auger widths of the KLL and KLM resonant states.

	KLL resonant			KLM resonant					
	$1s2s^2$	1s2s2p	$1s2p^2$	1s2s3s	1s2s3p	1s2s3d	1s2p3s	1s2p3p	1s2p3d
$\Gamma_r/\hbar\cdot s^{-1}$	8.46×10^{8}	1.85×10^{12}	4.10×10^{12}	9.81×10^{10}	7.84×10^{11}	3.41×10^{11}	1.96×10^{12}	6.13×10^{12}	6.80×10^{12}
$\Gamma_a/\hbar\cdot s^{-1}$	8.14×10^{13}	1.72×10^{14}	2.40×10^{14}	3.41×10^{13}	5.08×10^{13}	4.10×10^{12}	1.08×10^{14}	1.12×10^{14}	1.88×10^{13}
$(\Gamma_r/\Gamma)/\%$	0.001	1.06	1.68	0.29	1.52	7.69	1.79	5.20	26.57

4. Conclusions

In summary, we employ a new version of *R*-matrix computer programs (DARC) to study the PR process, based on a fully relativistic *R*-matrix and the close-coupling method. The method not only includes non-resonant recombination and resonant recombination, but also the interference effects between the two, naturally.

On the basis of this scheme, the partial and total PR cross sections of C V ion for incident-electron energies in the vicinity of the KLL and KLM resonant regions, and transition energies and probabilities from the KLL and KLM resonant states to the $1s^2nl$ ($n = 2$, 3, $l =$ s, p, d) states have been given in detail. Meanwhile, the principal resonant lines in each PR channel have also been identified in the present work. In order to test the correctness of the present calculations, we compare our composite PR cross sections to the high-resolution experimental measurements and available theoretical calculations, and a good agreement demonstrates the reliability of the present calculations. However, in the KLM resonant region, the present PR cross sections are overestimated due to the neglect of the radiation damping effect.

References

[1] Graham W G, Fritsch W, Hahn Y and Tanis J A 1992 *Recombination of Atomic Ions*, Vol. 269, in *NATO Advanced Study Institute, Series B: Physics* (New York: Plenum)
[2] Summers H P 1994 *Adv. At. Mol. Opt. Phys.* **33** 275
[3] Mason H E and Monsignori-Fossi B C 1994 *Astron. Astrophys. Rev.* **6** 123
[4] Wan J J and Dong C Z 2011 *Phys. Scr.* **84** 045301
[5] Pindzola M S, Robicheaux F J, Badnell N R, Chen M H and Zimmermann M 1995 *Phys. Rev. A* **52** 420
[6] Zhao L B, Ichihara A and Shirai T 2000 *Phys. Rev. A* **62** 022706
[7] Burke P G, Hibbert A and Robb W D 1971 *J. Phys. B* **4** 153
[8] Burke P G and Robb W D 1976 *Adv. At. Mol. Phys.* **11** 143
[9] Nahar S N and Pradhan A K 1991 *Phys. Rev. A* **44** 2935
[10] Nahar S N and Pradhan A K 1992 *Phys. Rev. Lett.* **68** 1488
[11] Nahar S N and Pradhan A K 1994 *Phys. Rev. A* **49** 1816
[12] Gorczyca T W, Robicheaux F, Pindzola M S and Badnell N R 1996 *Phys. Rev. A* **54** 2107
[13] Mitnik D M, Pindzola M S and Badnell N R 1999 *Phys. Rev. A* **59** 3592
[14] Zhang H L, Nahar S N and Pradhan A K 1999 *J. Phys. B* **32** 1459
[15] Pradhan A K, Chen G X, Nahar S N and Zhang H L 2001 *Phys. Rev. Lett.* **87** 183201
[16] Pradhan A K, Nahar S N and Zhang H L 2001 *Astrophys. J.* **549** L265
[17] Zhang H L, Nahar S N and Pradhan A K 2001 *Phys. Rev. A* **64** 032719
[18] Nahar S N and Pradhan A K 2004 *Radiat. Phys. Chem.* **70** 323

[19] Stancalie V 2013 *Eur. Phys.J.D* **67** 223
[20] Davies P C W and Seaton M J 1969 *J. Phys. B* **2** 757
[21] Knapp D A, Beiersdorfer P, Chen M H, Scofield J H and Schneider D 1995 *Phys. Rev. Lett.* **74** 54
[22] González Martínez A J, Crespo López-Urrutia J R, Braun J, Brenner G, Bruhns H, Lapierre A, Mironov V, Soria Orts R, Tawara H, Trinczek M, Ullrich J and Scofield J H 2005 *Phys. Rev. Lett.* **94** 203201
[23] Tobiyama H, Nohara H, Kavanagh A P, Nakamura N, Watanabe H, Sakaue H A, Li Y, Kato D, Currell F J, Yamada C and Ohtani S 2007 *J. Phys.: Conf. Ser.* **58** 239
[24] Nakamura N, Kavanagh A P, Watanabe H, Sakaue H A, Li Y, Kato D, Currell F J, Tong X M, Watanabe T and Ohtani S 2009 *Phys. Rev. A* **80** 014503
[25] Norrington P H 2004 www.am.qub.ac.uk/DARC
[26] Jönsson P, He X, Fischer F C and Grant I P 2007 *Comput. Phys. Commun.* **177** 597
[27] Grant I P 2007 *Relativistic Quantum Theory of Atoms and Molecules* (Berlin: Springer)
[28] Fritzsche S 2012 *Comput. Phys. Commun.* **183** 1525
[29] Kramida A, Ralchenko Y, Reader J and NIST ASD Team 2013 *NIST Atomic Spectra Database*, Ver. 5.1
[30] Heisenberg W 1925 *Z. Phys.* **32** 841
[31] Goudsmit S and Gropper L 1931 *Phys. Rev.* **38** 225
[32] Wölfli W, Stoller C, Bonani G, Suter M and Stöckli M 1975 *Phys. Rev. Lett.* **35** 656
[33] Salem S I, Kumar A, Soctt B L and Ayers R D 1982 *Phys. Rev. Lett.* **49** 1240
[34] Mannervik S, Asp S, Broström L, DeWitt D R, Lidberg J, Schuch R and Chung K T 1997 *Phys. Rev. A* **55** 1810
[35] Mu̇ller A, Schippers S, Phaneuf R A, Scully S W J, Aguilar A, Covington A M, Aĺvarez I, Cisneros C, Emmons E D, Gharaibeh M F, Hinojosa G, Schlachter A S and McLaughlin B M 2009 *J. Phys. B* **42** 235602
[36] Pradhan A K and Zhang H L 1997 *J. Phys. B* **30** L571
[37] Gu M F 2008 *Can. J. Phys.* **86** 675